
Investigation of the Difference Between Ordinary and FSI Numerical Solution for Flutter of Tandem Compressor

Alireza Sekhavat Benis and Reza Aghaei-Togh

Department of Aerospace Engineering, Science and Research Branch, Islamic Azad University, Tehran, Iran.

E-mail: reza_tog@srbiau.ac.ir

(Received 8 May 2023; accepted 23 October 2023)

This research aims to analyze and compare the flutter of turbine compressor blades from experimental, numerical, and fluid structure interaction (FSI) derived data. The results proved that the FSI solution results are closer to the experimental results. A reduced velocity parameter of 5 can be regarded as the flutter boundary in the bending flutter. Additionally, the incidence angle parameter equal to 1.5 can be characterized as the torsional flutter boundary. Tandem leads to strengthening the load applied on the compressor blades, reducing the number of compressor stages, and ultimately reducing the weight of the engine. Adding tandem to the rotor increases the vibration bending frequency by a factor of 2. Increasing the compressor velocity caused the FSI vibration frequency to be close to the experimental results. It was found that the vibration range of the main rotor is greater than that of the tandem. The vibration of the rotor and the tandem is damped for approximately 0.1 s to reach a constant frequency.

NOMENCLATURE

Chord (m)	C
Entropy (J)	H
Deformation gradient (m^3/s)	\hat{J}
Reduced velocity parameter	K
Mass (Kg)	m
Pressure (Pa)	P
Circumferential length of blade to blade (mm)	S
Temperature (K)	T
Circumferential length of front blade to rear blade (mm)	t
Flow velocity (m/s)	u
Differentiable deformation field	\hat{u}
Velocity of blade (m/s)	V
Reference volume (V)	\hat{V}
Axial distance (m)	X
Density (m/V)	ρ
frequency for bending flutter	ω
Axial overlap (m)	AO
Mean chord	C_{eff}
Incidence angle parameter	$f(i_m)$
interface of solid and fluid	$I(t)$
Leading edge	le
Percent pitch	PP
Trailing edge	te
symmetric stress tensor (Pa)	σ_f
Effective solidity	σ_{eff}
Front airfoil angle	φ_{FA}
Rear airfoil angle	φ_{AA}
Total chord angle	φ_{OV}

1. INTRODUCTION

Embedding a blade after the main blade in a turbomachine is termed tandem. The occurrence of tandem increases the pressure ratio in a compressor stage. As a result, the number of compressor stages can be reduced. Tandem technology increases the efficiency of the compressor stage by dividing the applied load between the main and rear blades. The load is divided equally on the blade and tandem. Correspondingly, by controlling the boundary layer, tandem wards off separation occurrence. Altogether, two effective factors in tandem include increased load applied on the stage and reduced engine weight.

In the study of turbomachines, flutter is a self-excited and undamped phenomenon caused by blade vibration. Often, this phenomenon is caused by the simultaneous function of elastic force, aerodynamic force, and inertial force on the blade. The flutter of the engine blades leads to severe damage to the blade structure in the short term, and a very challenging issue in aeroelasticity.

The mechanical coupling between two components at the collision point is realized as follows. The change in the shape of the structure caused by the applied forces of the fluid flow leads to a change in the fluid-structure interaction (FSI). This process causes a change in fluid conditions, which in turn changes the forces applied to the structure.

Simultaneous energy displacement between fluid and structure must be solved numerically. Coupled simulation can use a numerical solution to simultaneously solve the structure and fluid equations. It is also possible to use two independent programs for structure and fluid. The degree of complexity of numerical simulation depends on the problem, distance, and temporal discretization methods.

This study aims to investigate the flutter of a row of blades containing a tandem through the FSI approach.

2. LITERATURE REVIEW

Gezgüç¹ numerically evaluated the aerothermodynamics of the compressor tandem blade. They found that using tandem leads to reduced pressure drop and increased load factor. McGlumphy et al.² evaluated the compressor rotor tandem blades in three dimensions. The researchers found that the use of tandem makes the compressor more efficient than one with a single cascade. McGlumphy et al.³ evaluated tandem airfoils for axial-flow compressors numerically and compared the results with experimental data. Eshraqhi et al.⁴ evaluated the effects of the variable stator on tandem performance under high load in a three-dimensional and numerical mode. Tateishi et al.⁵ investigated the application of FSI methodology and modal technique for blade row flutter simulation. The researchers proved that the flow near the wall depends on the shock realization point and flutter characteristics.

Rajadurai et al.⁶ evaluated the conventional blade and blade with tandem rotor under the subsonic flow of the compressor in 2 dimensions and calculated the resulting response based on total pressure and static pressure. Mohsen et al.⁷ studied the effect of the NASA-37 rotor tandem blade on rotor performance under transonic flow in an axial compressor by numerical solution in 2 dimensions. They also set the Mach number equal to 1.4. The researchers concluded that tandem leads to the strengthening of flow circulation and its diffusion without flow separation and increases the pressure ratio and adiabatic efficiency of the rotor by 17% and 2%, respectively. Manas and Shine⁸ investigated the effects of geometrical parameters on the flow pattern in 2D and studied the effects of pressure drop on different modes.

Kumar⁹ studied the performance of tandem rotors in design and off-design modes and found that the tandem diffusion characteristic is better than the normal rotor. Wang et al.¹⁰ designed a row of the tandem blade in transonic flow and improved pressure and efficiency by 1.44% and 2.34%, respectively. Zhang¹¹ investigated the coupling effects between IGW (Inlet Guide Vane) and fan. The results showed that flutter is realized when the natural frequency of the structure is close to the transient frequency mode of the IGW. Pan et al.¹² evaluated the optimal design of a tandem blade under ultrasonic flow for NASA rotor 37 and studied the secondary flow and the resulting shock wave after the blade. Evaluations showed that the use of tandem leads to an increase in mass flow rate and surge margin and a decrease in efficiency. Efficiency and surge margin increased by 1.6% and 2.75%, respectively. The main reason for optimization is to reduce the three-dimensional effects of flow. As soon as the tandem is optimized, the flow from the trailing edge of the rotor tandem to the leading edge of the stator is optimized and the three-dimensional effects are significantly reduced.

Over the past few years, many numerical methods have been developed. However, the numerical method is very time-

Table 1. Rotor and tandem rotor geometry considerations.

Component	Value
Rotor tip diameter	At least 0.762 m (30 inches)
Hub/Tip ratio	0.7 to 0.8
Diffusion factor of the rotor tip	Less than 0.55
Rotor tip solidity	1.4 to 1.5

consuming due to the high volume and complexity of the calculations of the coupling method. To stabilize efficiency, researchers have recommended the unsteady aerodynamic reduction method. Su¹³ used the coupling method to investigate blade row flutter to obtain a powerful method. The results showed that the accuracy of the proposed method is two times higher than the usual methods. In one of the most recent research, Doroshenko et al.¹⁴ investigated the aeroacoustic parameters of a single-stage tandem (SST) compressor numerically using Navier-Stokes equations and introduced its advantages. The researchers finally concluded that the most suitable turbulence model for solving the tandem blade is the SST model. According to the mentioned research results, the use of tandem has increased the pressure ratio of the compressor between 1% and 15%. Also, this parameter has increased by 8.5% in the design mode. At the same time, the acoustic efficiency has been increased up to 3 % by using tandem. Tabatabaei et al.¹⁵ also studied the FSI in three dimensions for a rod. The researchers proved that the deformation of the rod increased by up to 90% between 0.25 and 0.35 m/s. Yuan Tao et al.¹⁶ numerically optimized the flow characteristics for the tandem rotor. The researchers concluded that the use of tandem reduces the pressure loss by 20% at the design point. Subsequently, they¹⁷ developed a new method for rapid optimization of blade design in subsonic flow in 2 dimensions.

Liu et al.¹⁸ increased the load applied to the axial compressor by using tandem blades. They defined parameter E as the limit of the compressor stall based on theoretical models, which indicates the capability of the tandem compressor to increase the applied load limit. The practical comparison of the normal stage with the tandem stage showed that the maximum efficiency increased by 1%. At the same time, the stall limit has also increased by 6%.

Babu et al.¹⁹ studied the secondary vortices of tandem rotors for axial compressors. The increase in energy caused by tandem reduces the amount of discontinuity and increases the rotation of the flow on the suction surface of the blade. This rotation of the realized flow after the rotor causes separation at the beginning of the stator. Also, the flow at different times was studied using the limited flow lines and the standardized Q level. The results showed that the transient flow is formed in the rotor after the tandem. Subsequently, the mixing of the rotor vortices with the leading edge of the stator forms new vortices at this point. The geometry adopted in this study is the same model evaluated at NASA Lewis Research Center.²⁰ Important considerations in the geometry of the problem are presented in Table 1.

Also, the following are considered in the geometry of the problem. (1) The geometry does not have any inlet guide vane

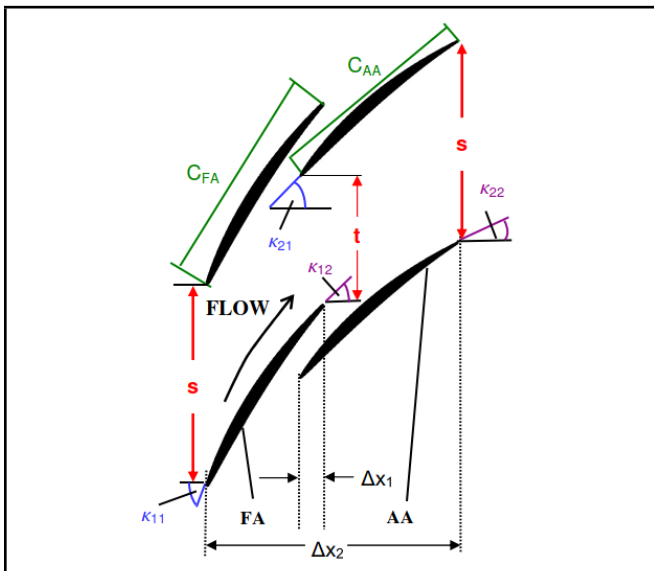


Figure 1. Stage geometry with tandem.²¹

Table 2. Geometric specifications of tandem stage.²²

Component	Value
Front airfoil chord angle	$\varphi_{FA} = K_{11} - K_{12}$
Rear airfoil chord angle	$\varphi_{AA} = K_{21} - K_{22}$
Total chord angle	$\varphi_{OV} = K_{11} - K_{22}$
Mean chord	$C_{eff} = (1 - 0.5 \cdot AO) \cdot s$
Effective solidity	$\sigma_{eff} = C_{eff} / s_{eff}$
Axial overlap	$AO = \Delta x_1 / \Delta x_2$
Percent pitch	$PP = t / s$

(axial inlet flow). (2) The flow at the output of the stator is axial. (3) The blade is double-arc-circular type.

As mentioned earlier, the tandem is equivalent to installing an additional blade behind the main blade. In general, the tandem behind the blade is the same as the flap on the wing. In fact, the key idea of the tandem is taken from the flap. The overall shape of the rotor under study is reflected in Fig. 1, inspired by NASA Lewis’s report.²⁰

The desired geometry is drawn in three dimensions in Fig. 2.

As soon as the desired geometry is drawn, a high-quality computational mesh is applied to the desired geometry.

3. COMPUTATIONAL MESH

After creating the geometry of the compressor stage, the computational mesh was developed based on the quality and the mesh independence (Fig. 3).

4. BOUNDARY CONDITIONS

The following boundary conditions were included in all simulations of this study. (A) Total pressure and temperature were used for stage input. The total pressure was equal to 1 atmosphere and the total temperature was equal to 288 K. (B) All walls i.e. blade, shell, and root were considered without roughness. (C) The averaged static pressure was used in the output.

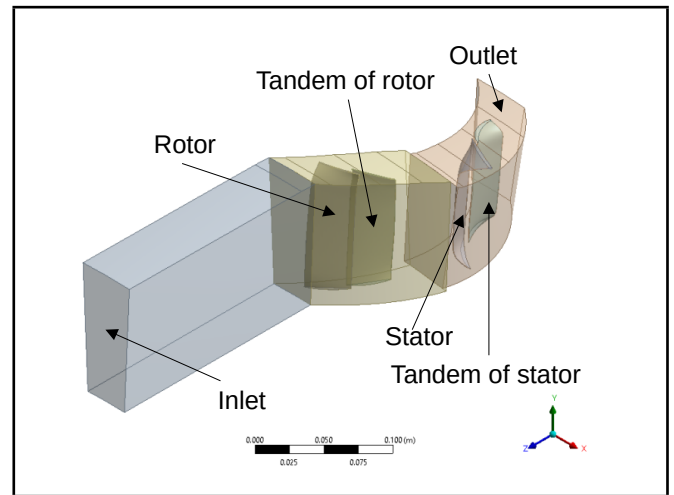


Figure 2. 3D geometry under study.

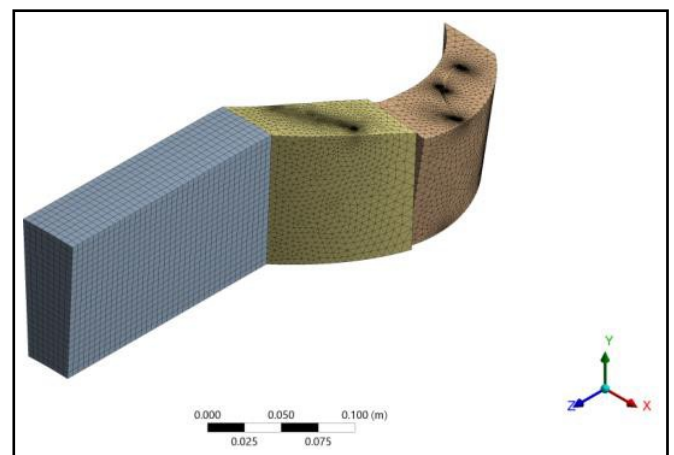


Figure 3. Mesh drawn on geometry.

Two channels of the rotor and stator were modeled separately. The equations have been solved using the time transformation method. To obtain the stage performance curve, the outlet pressure was continuously increased until a numerical instability was observed.

5. COMPUTATIONAL MESH AND ITS VERIFICATION

According to Fig. 4, as soon as the number of nodes decreased, the value of the rotor pressure ratio came closer to its nominal value (1.28) (reported in NASA Lewis²⁰). By increasing the number of nodes from mesh number 1 to 3, a relatively large change in the value of the pressure ratio was realized. But as the number of nodes increased from mesh number 4 to 5, the rotor pressure ratio did not change much and remained almost constant. To reduce the computational cost, mesh 4 was used for analysis, because the results of this mesh were independent of the number of computing nodes.

To verify the results, the pressure ratio obtained from the experimental results of the Lewis NASA report²⁰ was compared with the three-dimensional analysis of the present research in Fig. 5. Where in experiments, air entered the compressor through a 31.4 m combined inlet duct, plenum, and

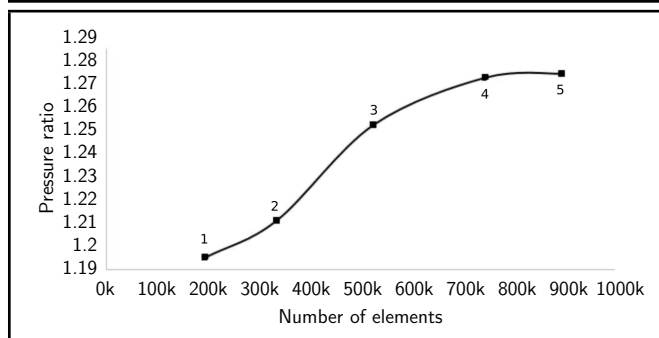


Figure 4. Computational meshes under study

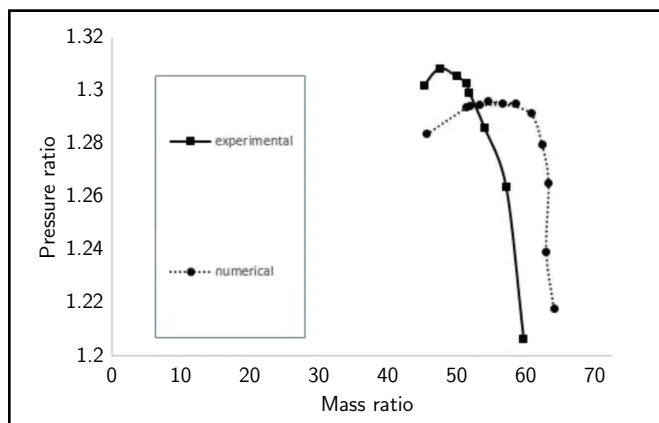


Figure 5. Comparison of pressure ratio obtained from experimental and numerical solutions.

bellmouth inlet, and was exhausted through an exit diffuser to the atmosphere ($P = 1$ atm and $T = 273$ K). The pressure ratio was set between 1.2 to 1.32, the velocity was set between 0.4 to 0.6 Mach and $N = 4210$ rpm.²⁰ The insignificant difference caused by the flow rate was more in the numerical results. The reason was that the friction in the numerical analysis was lower than the level of friction in the experimental results, which in turn is due to the lack of mention of friction in the report.²⁰ Also for a qualitative comparison, it can be seen that the peak for experimental curve occurred sooner and in low mass ratios than numerical curve, the reason was that in experimental study there was friction and redundant vortices (which had not been investigated in numerical studies (that makes the mass ratio much fewer. Also the peak of the experimental line²⁰ was higher than numerical one, that is because in experiments, there was friction and redundant vortices that made the flow loose pressure and the pressure ratio became higher. Also in figure 5 it can be seen that in pressure ratio 1.26, mass ratio for experimental data was 58 kg/s and for numerical data was 63 kg/s, that shows 8.6% error (which is acceptable).

6. RESEARCH METHODOLOGY

The research method of this study was based on numerical methodology. In this regard, first only the desired geometry data were drawn. Both rotor and stator had the tandem capability. As mentioned before, compressor stages were Hub/Tip type. Each stage was realized in the form of a rotor plus tandem and a stator plus tandem (in the form of two airfoils in a

row). The main blade and tandem rotor were designed to produce a pressure ratio of 1.28 at a speed of 230 m/s (757 ft/sec). The stage pressure ratio at the design velocity was 1.26 for both stages. Adiabatic efficiency for the rotor and the whole stage at the design velocity was 90% and 85%, respectively. The use of tandem lead to an increase in pressure ratio and efficiency compared to normal blades. Also, the aerodynamic load distribution between the blade and the tandem lead to a decrease in the three-dimensional flow near the walls. The values of reduced velocity and the angle parameter for the rotor were calculated positive and negative angles from 50% to 110% of the design velocity, respectively, as follows:²⁰

$$K = \frac{12 V}{\pi c \omega}; \quad (1)$$

$$f(i_m) = \frac{i_m - i_{m_{ref}}}{\text{low} - \text{loss incident range}}; \quad (2)$$

where the values of V , c , $i_{m_{ref}}$, and low-loss incident range were extracted from the airfoil parameters located at 25% span from the tip. Also, bending and torsional flutters were calculated at Mach numbers 0.4 and 0.6.

7. FLUID-STRUCTURE INTERACTION

The fluid and structure coupling realized by boundary conditions at the incidence level $I(t)$ (definition of the interface of solid and fluid) can be expressed by the simple laws of physics:

Movement conditions: Fluid and structure velocity variables were continuous on the incidence surface.

Dynamic conditions: Stresses perpendicular to the fluid and structure are continuous at the incidence surface

Geometric conditions: fluid and structure domains must match. The domains should not overlap and a gap should not appear.²³

The included conditions can be considered as boundary conditions sub-problems.

7.1. The Solids Problem

In the study of fluid-structure interaction, the Lagrange reference system was used to evaluate the dynamics of the elastic structure. The momentum equation can be expressed as follows:²³

$$\hat{J} \hat{\rho} \partial_{tt} \hat{u} = \hat{J} \hat{\rho} \hat{f} + \hat{\text{div}}(\hat{F} \hat{\Sigma}). \quad (3)$$

Conservation of mass was also formulated as follows:²³

$$m(\hat{V}) = \int \hat{\rho}^0(\hat{x}) d\hat{x} = \int \hat{J} \hat{\rho}(\hat{x}, t) d\hat{x}. \quad (4)$$

The general problem of elastic structure at the Lagrangian origin \hat{V} was formulated as follows:²³

$$\hat{\rho}^0 \partial_{tt} \hat{u} - \hat{\text{div}}(\hat{F} \hat{\Sigma}) = \hat{\rho}^0 \hat{f}. \quad (5)$$

7.2. The Fluids Problem

The complete Navier–Stokes equations were as follows:²³

$$\rho_f(\partial_t v + (V \cdot \nabla)v) - \text{div}\sigma = \rho_f f; \quad \text{div}V = 0. \quad (6)$$

Applying the material law to the Navier–Stokes equation of fluid, we have:²³

$$\rho_f(\partial_t v + (V \cdot \nabla)v) + \nabla p - \rho_f \nu_f \text{div}(\nabla v + \nabla v^T) = \rho_f f; \quad \text{div}V = 0. \quad (7)$$

And the reduced formulation was outlined as follows:²³

$$\rho_f(\partial_t v_f + (V \cdot \nabla)v) - \rho_f \nu_f + \nabla p = \rho_f f; \quad \text{div}V = 0. \quad (8)$$

To investigate fluid-structure interaction, the role of boundary stresses is very important for the coupling fluid and structure. For this reason, the symmetric stress tensor σ_f should be considered. One of the coupling conditions is the coupling of the vertical stresses of the fluid problem and the solid problem.²³

$$n \cdot \sigma_f = n \cdot \sigma_s. \quad (9)$$

In the above equation, σ_s was replaced by Cauchy stress tensor:²³

$$\sigma_f = \hat{J}^{-1} F \hat{\Sigma}_S \hat{F}^T. \quad (10)$$

After placement, we have:²³

$$-pn + \rho_f \nu_f n \cdot (\nabla v + \nabla v^T) = n \cdot \sigma_S; \quad (11)$$

or

$$-pn + \rho_f \nu_f n \cdot \nabla v = n \cdot \sigma_S. \quad (12)$$

7.3. Movement Conditions

The movement coupling was such that the viscous fluid sticks to the solid boundary.²³

$$v_f(x, t) = v_S(x, t) \text{ on } I(t). \quad (13)$$

We needed to find a way to combine the fluid velocity $v_f(x_i, t)$ with the solid velocity $\hat{v}_s(\hat{x}_i, t) = d_t \hat{u}_s(\hat{x}_i, t)$ at the intersection point $x_i \in I(t)$. This integration was realized by using the mapping solid deformation properties $x_i = \hat{x}_i + \hat{u}_s(\hat{x}_i, t)$ which expressed the association between Lagrangian and Eulerian coordinates. This mapping was realized as $\hat{T}_s(\hat{x}_i, t) := \hat{x} + \hat{u}_s(\hat{x}, t)$. Subsequently, the coupling of movement conditions is also formulated as follows:²³

$$v_f \circ T_s = \hat{v}_S \text{ on } \hat{I}. \quad (14)$$

For the current situation, we have:²³

$$v_f = \hat{v}_S \circ \hat{T}_s^{-1} \text{ on } I(t). \quad (15)$$

For each $\hat{x}_i \in \hat{I}$ the following conditions must apply:²³

$$v_f(\hat{x}_i + \hat{u}_s(\hat{x}_i, t)) = \hat{v}_s(\hat{x}_i, t). \quad (16)$$

Equation (16) represents the nonlinearity of the movement coupling conditions.²³

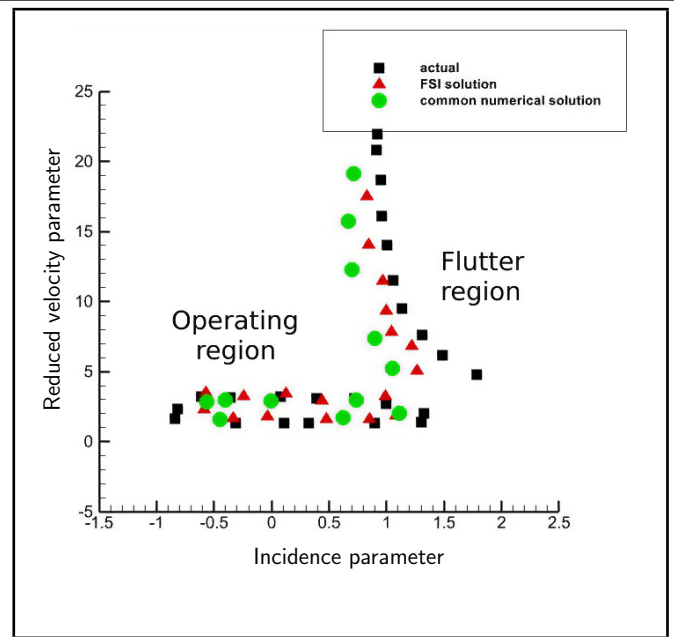


Figure 6. Reduced velocity parameter regarding the angle of attack parameter related to the first bending flutter at Mach number 0.4 for tandem rotor.

8. SOLVING THE PROBLEM CONSIDERING FSI

Figure 6 reflects the reduced velocity parameter regarding the angle of attack parameter associated with the first bending flutter at Mach number 0.4. As shown in the figure, the symbol “square” represents the behavior of the tandem rotor in experimental (actual) conditions. According to the figure, the number 5 in the reduced velocity parameter can be the boundary between normal operating and operating flutter. A comparison of the operating flutter resulting from the normal solution with the FSI-based solution shows that the FSI solution is more like the normal solution. The reason is that the FSI solution provides a better answer by modeling unbounded fluid and structure incidences. Finally, the error of the normal solution is more compared to the FSI solution. This error is caused by not including the fluid and structure interaction in the calculations. On the other hand, bending flutter is achieved at a lower speed than torsional flutter. Also, as the angle of attack increases, flutter of the tandem rotor occurs at a lower speed. As can be seen, the FSI method can predict flutter by less than 0.1-degree error in incidence parameter and ordinary numerical solution has about 0.4-degree error; thus the FSI method has more than 75% accuracy in predicting the flutter than the ordinary numerical solution. Finally, the reduced velocity parameter is defined in equation 1.

Figure 7 shows the reduced velocity parameter regarding the angle of attack parameter associated with the first torsional flutter at Mach number 0.6. According to the figure, the FSI solution is closer to the experimental (actual) solution (which is derived from NASA’s report²⁰) than the normal solution (not using the FSI method in numerical solution). This shows the priority, superiority, and prediction of flow by the FSI. As shown in the figure, as the angle of attack increases, flutter

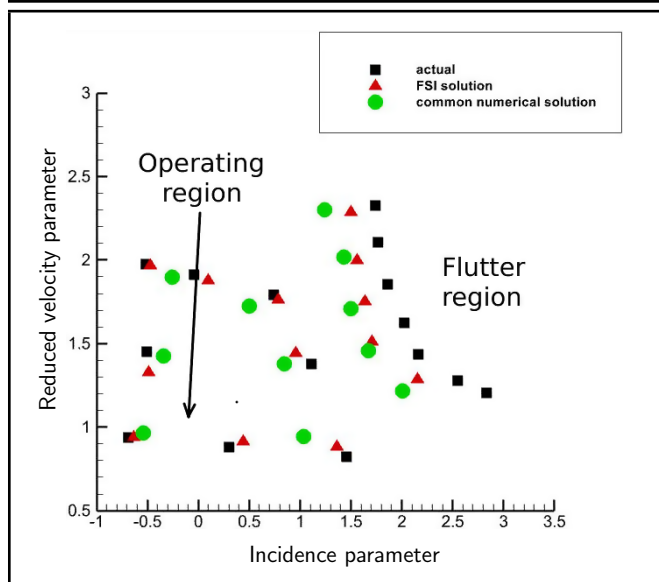


Figure 7. Reduced velocity parameter regarding the angle of attack parameter related to the first torsional flutter at Mach number 0.6 for tandem rotor.

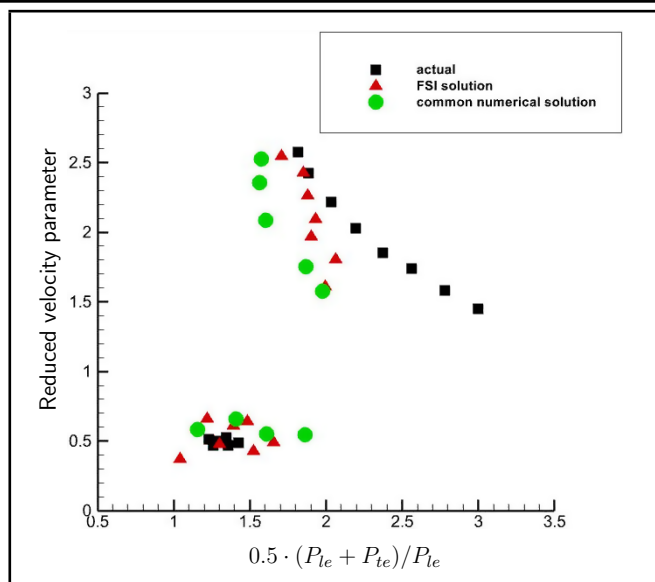


Figure 9. Average pressure ratio regarding reduced velocity parameter related to torsional flutter for the rear stator (tandem).

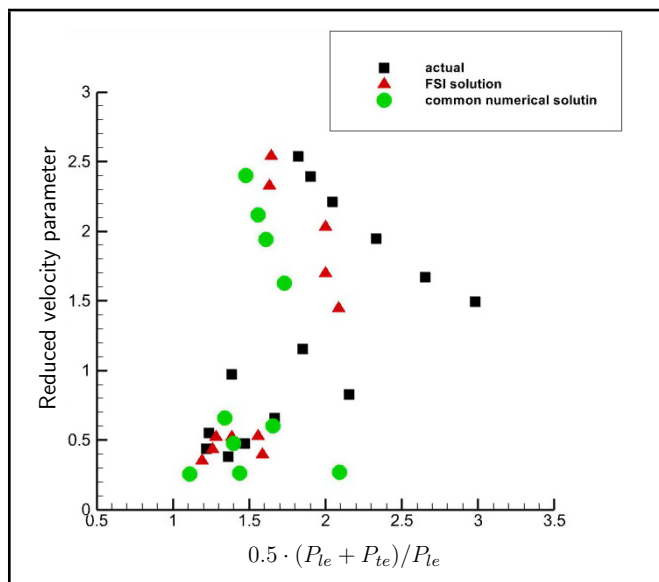


Figure 8. Average pressure ratio regarding reduced velocity parameter related to torsional flutter for the front stator (main).

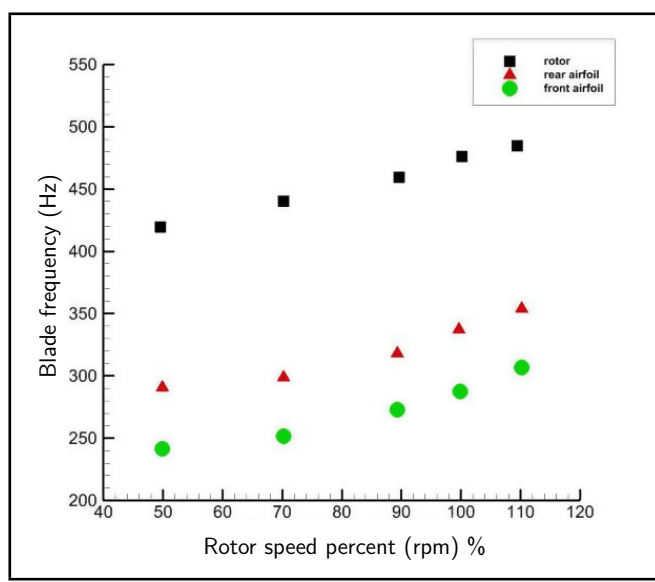


Figure 10. Resonance frequency of the main rotor, tandem rotor, and the total region of the rotor (main rotor and tandem rotor) regarding its rotation speed.

bending occurs at a lower speed. On the other hand, torsional flutter is realized at a lower speed than bending flutter. At the same time, the normal solution can predict flutter at a lower speed and angle of attack than the experimental solution. This result indicates the incompatibility of this solution with the FSI solution that observes the fluid and structure interaction. The Fig. 7 showed that the FSI solution has more than 70% accuracy in comparison with the ordinary solution method to predict the blade and tandem flutter.

Figures 8 and 9 show the average pressure ratio regarding the reduced velocity parameter for the front (main) and rear (tandem) stators for torsional flutter. As can be seen in the figures, the FSI solution is more like the experimental solution. At the same time, the normal solution can show the amount of flutter in the speed and average pressure ratio higher than the experimental solution. As it is shown in Fig. 8, for re-

duced velocity parameter 2, average pressure ratios for actual, the FSI and common numerical solutions are 2.3, 2.05 & 1.6. It is obvious that the FSI method has more than 35% accuracy compared with ordinary numerical solution to predict flutter. For both figures it is obvious that as the reduced velocity parameter decreases and average pressure ratio increases, error of the FSI method increases and the accuracy decreases.

Resonance frequency of the main rotor, tandem rotor, and the total region of the rotor (main rotor and tandem rotor) regarding its rotation speed is shown in Fig. 10. In 100% rotor speed, resonance frequency of rotor (front airfoil) is 270 Hz (green circle), while by adding tandem (rear airfoil), the resonance frequency of the whole rotor becomes 465 Hz (black square). Which means by adding tandem, the resonance frequency increases 1.72 times.

The displacement of rotor and tandem is discussed in

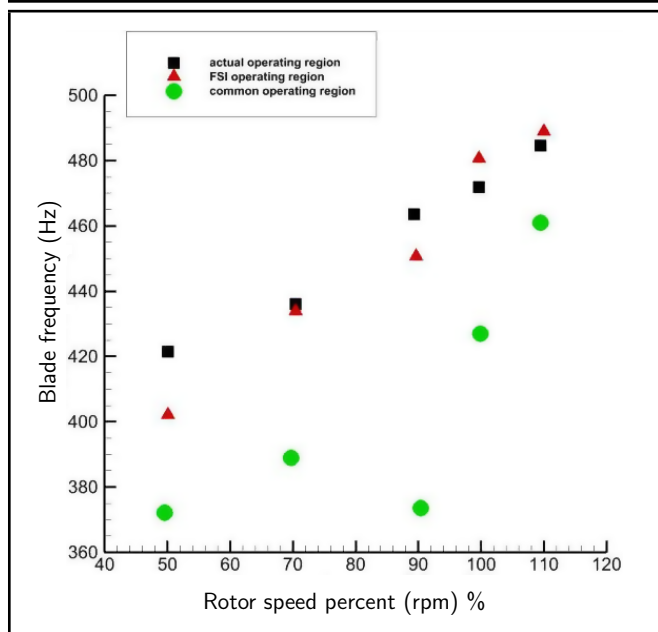


Figure 11. Bending frequency of the rotor blade.

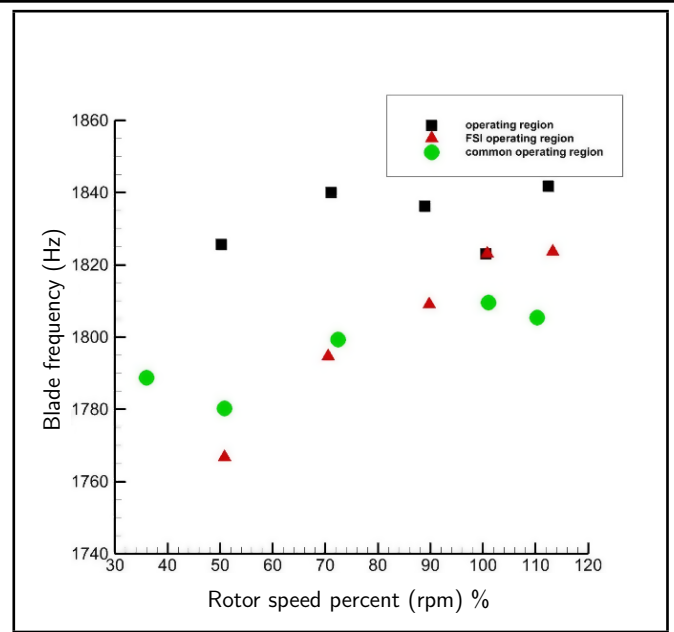


Figure 13. Bending frequency of the stator blade.

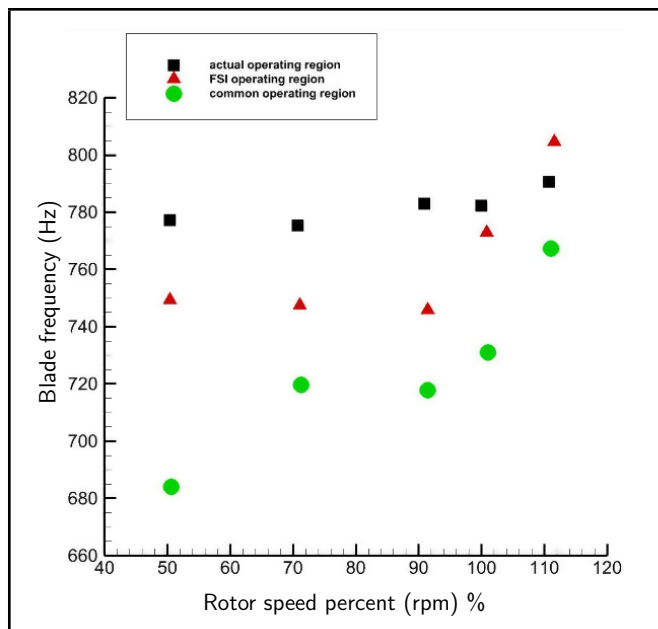


Figure 12. Rotation frequency of the rotor blades.

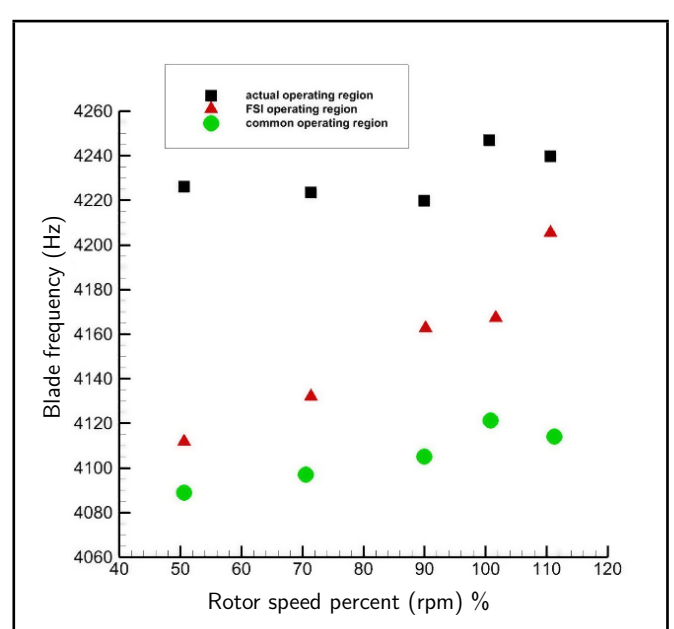


Figure 14. Rotation frequency of the stator blade (rotation frequency of the compressor $N = 4210$ rpm).

Figs. 15 & 16. While for further studies, investigation of the displacement of rotor and tandem by details will be studied in future works.

Figure 11 shows the bending frequency of the rotor blade in experimental conditions, numerical solution, and numerical solution based on the FSI. As shown in the figure, the numerical solution based on the FSI has a lower error compared to the normal numerical solution and can predict the flow movement well. In the normal numerical solution, the interaction between fluid and structure is not considered. As a result, despite the prediction of flow, it imposes a large error compared to the numerical solution based on the FSI. Also, as the compressor speed increases, the difference between the FSI solution and the experimental answer decreases. The reason is that increasing the speed of the compressor leads to the strength-

ening of vibration and incidences between fluid and structure, which in turn increase the range of blade vibration. Therefore, the FSI solution can calculate the incidence between the blade and the other components well.

The rotation frequency of the rotor blade is reflected in Fig. 12. As shown in the figure, the numerical solution of the FSI is the closest to the experimental solution. Also, the normal numerical solution has the highest error compared to the numerical solution based on interaction fluid and structure. As mentioned earlier, the FSI solution handles fluid and structure incidences well. Therefore, more interaction leads to higher compressor rotation speed and the data obtained from the FSI solution is more accurate.

Figure 13 reflects the bending frequency of the stator blade

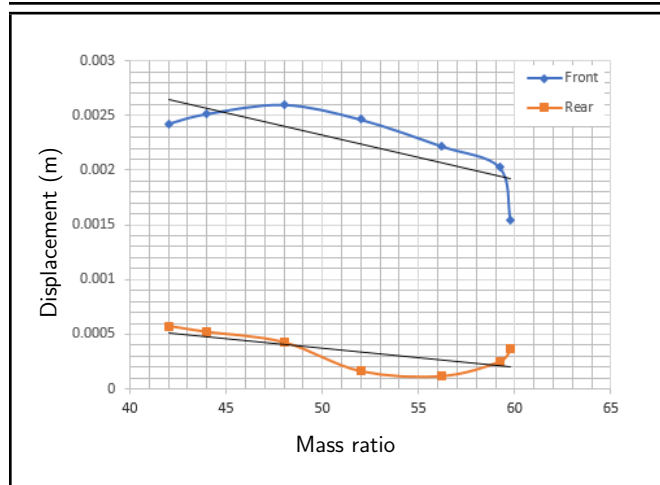


Figure 15. Comparison of normal and tandem rotors displacement regarding the mass ratio ($N = 4210$ rpm).

in different solutions. The results of both the FSI and experimental solutions are very close to each other. Since the FSI solution handles the increased flow compressor speed, increasing the compressor speed makes the FSI solution closer to the experimental data.

The rotation frequency of the stator blade is reflected in Fig. 14. According to the figure, the FSI numerical solution has less error than the normal numerical solution. As the rotation speed increases, the error of the numerical solution based on the fluid and structure interaction decreases compared to the experimental solution.

In Fig. 15, the displacement of blades regarding mass ratio is reflected. As shown in the figure, the displacement of the main blade and tandem blade is equal to 0.0009 and 0.0005 meters, respectively. The reason for the greater displacement of the main blade compared to the tandem blade is that the flow hits the main blade in a confused manner and increases the vibration of this blade. On the opposite point, the tandem blade receives a flow of the main blade with fewer disturbances and tolerates less displacement.

To achieve more accuracy in the study, the time step is set equal to 0.0001 and the solution is achieved by the unsteady method. As shown in Fig. 16, the vibration range of the main rotor is initially very high. Gradually, the range of the vibration is reduced but not damped. Finally, the vibration stabilizes in a certain range. The oscillation rate of the tandem blade is high at the beginning. However, the range of oscillation gradually decreases, and it vibrates in a certain range. The tandem blade vibrates at a lower range than the main blade. The reason is that initially; the flow hits the main rotor in a confused manner. However, after passing through the main blade, the amount of flow disturbance is much less, and the blade vibration is reduced.

9. CONCLUSION

The purpose of this article is to study tandem blade flutter considering the FSI. All the illustrative diagrams show that the results of the FSI solution are closer to the experimental results

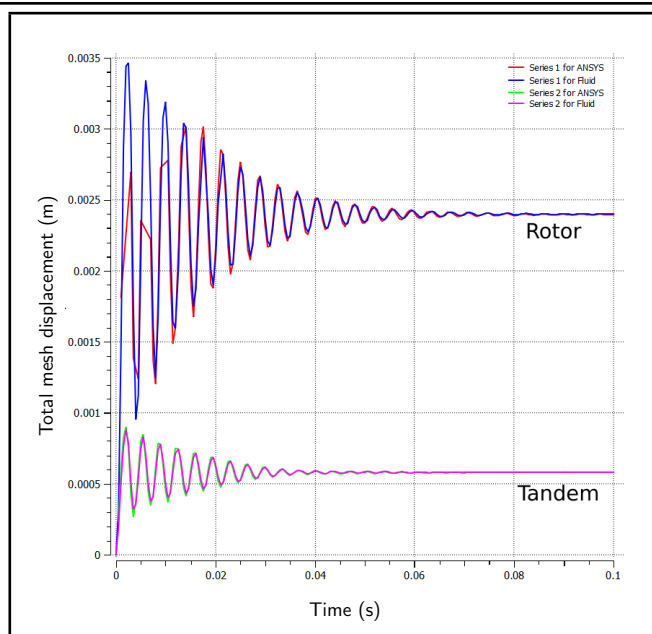


Figure 16. Rotor vibration range and its tandem regarding time.

than the numerical solution (not using the FSI method). In each diagram of reduced velocity regarding the incidence angle, two separate regions called normal operation and flutter operation have been formed. For the first bending flutter of the rotor, the reduced velocity parameter of 5 is the flutter boundary. For the first torsional flutter, the incidence angle of 1.5 is the flutter boundary. Also, in the diagram of the pressure ratio regarding the reduced velocity parameter, two separate regions, i.e., normal operation and flutter operation have been formed for the stator and its tandem. The use of tandem in the rotor increases the vibration frequency by 2 times. In addition, increasing the speed of the compressor increases the similarity of the results of the FSI solution to the experimental results. The vibration amplitude of the tandem is not damped and less than the vibration amplitude of the main rotor, due to the reduction of the flow disturbance passing through the main rotor.

REFERENCES

- Gezguç, C. Numerical study of axial compressor tandem blade aerothermodynamic performance, *22nd International Symposium on Air Breathing Engine*, (2015)
- McGlumphy, J., Ng, W. F., Wellborn, S. R., Kempf, S., Numerical Investigation of Tandem Airfoils for Subsonic Axial-Flow Compressor Blades, *Journal of Turbomachinery-Transactions of The Asme*, **131**(2), 021018 (2009) <https://doi.org/10.1115/1.2952366>
- McGlumphy, J., Ng, W. F., Wellborn, S. R., Kempf, S., 3D Numerical Investigation of Tandem Airfoils for a Core Compressor Rotor, *Journal of Turbomachinery-Transactions of The Asme* **132**(3): 031009 (2010), <https://doi.org/10.1115/1.3149283>

- ⁴ Eshraghi, H., Boroomand, M., Tousi, A. M., Fallah, M. T., Mohammadi, A., The effect of variable stator on performance of a highly loaded tandem axial flow compressor stage, *Journal of Thermal Science*, **25**, 223–230. (2016), <https://doi.org/10.1007/s11630-016-0854-y>
- ⁵ Tateishi, A., Watanabe, T., Himeno, T., Aotsuka, M., Murooka, T., Verification and Application of Fluid-Structure Interaction and a Modal Identification Technique to Cascade Flutter Simulations. *International Journal of Gas Turbine, Propulsion and Power Systems*, **8**(3), 20–28. (2016). https://doi.org/10.38036/jgpp.8.3_20
- ⁶ Rajadurai, M., Vinayagam, P., Balakrishnan, K., Priya, G. M., 2-D Numerical Investigation of the Single Blade and Tandem Blade Rotor in Low Speed Axial Flow Compressor *International Journal of Computational Engineering Research*, **7**(6), 56–64. (2017).
- ⁷ Mohsen, M., Owis, F. M., Hashim, A. A. The impact of tandem rotor blades on the performance of transonic axial compressors. *Aerospace Science and Technology*, **67**, 237–248. (2017). <https://doi.org/10.1016/j.ast.2017.04.019>
- ⁸ MP, M. (2022). Characterization of Tandem Airfoil Configurations of Axial Compressors. *International Journal of Turbo & Jet-Engines*, **39**(2), 167–181. <https://doi.org/10.1515/tjj-2018-0018>
- ⁹ Kumar, A., Pradeep, A. M. Performance evaluation of a tandem rotor under design and off-design operation. In *Turbo Expo: Power for Land, Sea, and Air* (Vol. **50992**, p. V02AT39A009). American Society of Mechanical Engineers. (2018).
- ¹⁰ Yue, S., Yangang, W., Haitong, W., Design and Optimization of Tandem Arranged Cascade in a Transonic Compressor. *Journal of Thermal Science*, **27**, 1–10. (2018). <https://doi.org/10.1007/s11630-018-1013-4>
- ¹¹ Zhang, W., Xu, Y., Su, D., Gao, Y. Flutter Analysis of Tandem Cascades Based on a Fluid-Structure Coupling Method. *Journal of Aerospace Engineering*, **32**(2), 04018147. (2019). [https://doi.org/10.1061/\(ASCE\)AS.1943-5525.0000975](https://doi.org/10.1061/(ASCE)AS.1943-5525.0000975)
- ¹² Pan, R., Song, Z., Liu, B., Optimization design and analysis of supersonic tandem rotor blades. *Energies*, **13**(12), 3228. (2020). <https://doi.org/10.3390/en13123228>
- ¹³ Su, D., Zhang, W., Ye, Z. A reduced order model for uncoupled and coupled cascade flutter analysis. *Journal of Fluids and Structures*, **61**, 410–430. (2016). <https://doi.org/10.1016/j.jfluidstructs.2015.11.013>
- ¹⁴ Doroshenko, E.V., Tereshchenko, Y.M., Tereshchenko, Y.Y., Kushchinskiy, A.O., Aeroacoustic characteristics of the axial compressor stage with tandem impeller, *Dnipropetrovsk Iss.* **1**, (2019) 48–54. <https://doi.org/10.29202/nvngu/2019-1/9>
- ¹⁵ Tabatabaei Malazi, M., Eren, E.T., Luo, J., Mi, S., Temir, G., Three-Dimensional Fluid-Structure Interaction Case Study on Elastic Beam *J. Mar. Sci. Eng.* **8**, 714. (2020). <https://doi.org/10.3390/jmse8090714>
- ¹⁶ Tao, Y., Wu, Y., Yu, X., & Liu, B. Analysis of Flow Characteristic of Transonic Tandem Rotor Airfoil and Its Optimization. *Applied Sciences*, **10**(16), 5569. (2020). <https://doi.org/10.3390/app10165569>
- ¹⁷ Tao, Y., Yu, X., Liu, B., A New Method for Rapid Optimization Design of a Subsonic Tandem Blade. *Applied Sciences*, **10**(24), 8802. (2020). <https://doi.org/10.3390/app10248802>
- ¹⁸ Baojie, L.I.U., Zhang, C., Guangfeng, A.N., Du, F.U., Xianjun, Y.U. Using tandem blades to break loading limit of highly loaded axial compressors. *Chinese Journal of Aeronautics*, **35**(4), 165–175. (2022). <https://doi.org/10.1016/j.cja.2021.07.031>
- ¹⁹ Babu, S., Chatterjee, P., Pradeep, A.M., Transient nature of secondary vortices in an axial compressor stage with a tandem rotor. *Physics of Fluids*, **34**(6). (2022); <https://doi.org/10.1063/5.0092226>
- ²⁰ Brent, J.A., Cheatham, J.G., Clemmons, D.R., *single-stage experimental evaluation of tandem-airfoil rotor and stator blading for compressors, part v - analysis and design of stages d and e*, pratt & whitney aircraft, division of united aircraft corporation, florida research and development center, prepared for national aeronautics and space administration, NASA Lewis Research Center, Contract NAS3-11158. (1972)
- ²¹ Shamsodini Lori, R., Tusi, A.M., Eshraghi, H., Transient Numerical Analysis of a Tandem Compressor Stage *Amirkabir Journal of Mechanical Engineering*, **51**(2) 117–119, (2019) (in Persian) <https://doi.org/10.22060/mej.2017.12446.5338>
- ²² Yue, S., Wang, Y., & Wang, H. Design and optimization of tandem arranged cascade in a transonic compressor. *Journal of Thermal Science*, **27**, 349–358. (2018). <https://doi.org/10.1007/s11630-018-1013-4>
- ²³ Richter, T. *Fluid-structure interactions: models, analysis and finite elements* (Vol. 118). Springer. (2017).